



Research Article

# Flow behavior of thermo-thickening associative polymers in porous media: effects of associative content, salinity, time, velocity, and temperature

Siv Marie Åsen<sup>1</sup> · Arne Stavland<sup>2</sup> · Daniel Strand<sup>2</sup>

Received: 30 September 2021 / Accepted: 17 January 2022

Published online: 14 February 2022

© The Author(s) 2022 **OPEN**

## Abstract

Above a critical temperature, thermo-thickening associative polymers (TAPs) have a superior ability to decrease the mobility of the water phase, compared to traditional polymers for enhanced oil recovery. The ability to decrease the mobility, will be amplified at low flow velocities, and by the presence of salt, and is much higher in porous media than would be expected from bulk viscosity. In this work, we have examined TAPs ability to reduce the mobility, i.e., to increase the resistance factor. We have studied the effect of increasing the associative content, changing the porous media, changing the salinity, and scaling up the size of the porous media. How the resistance factor evolved, was studied as a function of temperature, velocity, and time. We found that a critical associative content or critical concentration of polymer was needed to achieve thermo-thickening in the porous media. As expected, thermo-thickening increased by increasing the salinity. For the relative homogenous clastic porous media investigated here, ranging from ~ 1 Darcy sandstone to multi-darcy sand, type of porous media did not seem to have a significant impact on the resistance factor. Time and amount of polymer injected is a critical factor: The buildup of thermo-thickening is delayed compared to the polymer front. For our tests with the weaker systems, we also observed a breakdown of the associative network at very low injection rates, possibly caused by the formation of intramolecular association.

## Article highlights

### Key findings from our tests of thermo-thickening associative polymer for enhance oil recovery operations:

- At high temperature, the polymer solutions mobility in porous media is much lower than expected from viscosity
- At low temperature, the flow behavior is like that of a traditional synthetic polymer
- This will mean good injectivity and superior sweep, compared to a traditional polymer for enhanced oil recovery

**Keywords** Thermo-thickening associative polymers · Enhanced oil recovery · Mobility reduction · Resistance factor · Scale effects · Time effects

✉ Siv Marie Åsen, [sias@norceresearch.no](mailto:sias@norceresearch.no) | <sup>1</sup>Department of Energy Resources, University of Stavanger, Stavanger, Norway. <sup>2</sup>NORCE Energy, NORCE Norwegian Research Centre AS, Stavanger, Norway.



SN Applied Sciences

(2022) 4:78

| <https://doi.org/10.1007/s42452-022-04961-w>

SN Applied Sciences  
A **SPRINGER NATURE** journal

## 1 Introduction

In polymer enhanced oil recovery (EOR) operations, polymer is added to the water phase to increase the viscosity and thereby reduce the mobility of the displacing fluid. When the mobility ratio of the displacing fluid (water) to the displaced fluid (oil) is decreased, sweep is improved, water break through is delayed and oil production is accelerated. A detailed description of the mechanisms improving the sweep can be found in Sorbie [31] and has been revised by several authors, including Standnes and Skjevrak [32] in their literature review, reporting 50 years of polymer pilots and field cases.

According to Sheng et al. [30], polymer flooding is the most widespread method for enhanced oil recovery by chemicals. Standnes and Skjevrak [32] inform that of the 72 projects described in the literature, only 6 were deemed discouraging. Despite their proven success, traditional synthetic EOR-polymers have their drawbacks: Sorbie [31] state that high molecular weight is needed for high viscosity and Stavland et al. [33] report that low molecular weight is desired to minimize mechanical degradation and ensure injectivity. As for most fluids, viscosity of traditional polymer solutions decreases with increasing temperature [14, 23]. Furthermore, viscosity is reduced in the presence of salt, and so is the mechanical stability [2, 22, 34]. Polymeric solutions for EOR are non-Newtonian fluids, and shear-thinning. In porous media, above a critical elongation rate, synthetic polymers tend to become shear-thickening and at an even higher shear rates, the polymer molecules are irreversibly degraded (see e.g. [2, 19, 22, 27, 33]).

An ideal polymer candidate for EOR would be one with a low resistance to flow at the high shear rates close to the injector and a high resistance to flow at the in-depth shear rates. The concept of reversible thermo-thickening associative polymers, first described by Hourdet et al. [14], and elaborated by L'Alloret et al. [16], Durand and Hourdet [10], Durand and Hourdet [11] seems to possess many of the properties favorable for polymer EOR.

Thermo-thickening associative polymers (TAPs) are co-polymers composed of a water-soluble main polymer and a low fraction of relatively small segments of a polymer with lower critical solution temperature (LCST) in water. Polymers with LCST will, when they are not part of a TAP, have a solubility that, contradictory to the common behavior, decreases with increasing temperature. That is, the polymer changes from a hydrophilic to a hydrophobic polymer as temperature increase. Below its LCST, the polymer will be completely miscible in water and above it will start to phase separate.

Due to the hydrophilic to hydrophobic transition of the incorporated segments as temperature increases, a TAP will, at low temperature, behave like the water-soluble main polymer and at higher temperature it will act as a hydrophobically associating polymer. Interactions between the now hydrophobic segments on different polymer molecules, will form a weak gel-like structure with increased resistance to flow. That is, the viscosity of the TAP will increase with increasing temperature. L'alloret et al. [16] and Zhu et al. [38] report that the thickening effect is strongly shear-thinning.

As of today, over 70 non-ionic polymers with LCST have been identified. Examples and chemical structure can be found in Cao et al. [5] and L'Alloret et al. [16]. According to L'Alloret et al. [16] conceptually, all these thermosensitive polymers can be incorporated as segments into a water-soluble polymer as block-units or side chains to create a TAP. And, as stated by L'alloret et al. [16], Durand and Hourdet [10] and Durand and Hourdet [11] the on-set of thermo-thickening will be dictated by the thermodynamical behavior of the incorporated segments. Several authors, including L'alloret et al. [16] and Grinberg et al. [13] report reduction of LCST with increased salinity and according to Du et al. [7] the salt depression of LCST follows the Hofmeister series. Consequently, the temperature for onset of thermo-thickening for a TAP will decrease with increasing salinity. Reichenbach-Klinke et al. [26] report that the magnitude of thickening in porous media is also improved by salinity.

In this work we have studied porous media behavior of one type of TAP with varying amount of the LCST-polymer (i.e. varying associative content) at different temperatures and salinities. Because, even if it is possible to measure thermo-thickening of TAPs in bulk by measuring rheologic properties (shear dependent viscosity, elastic properties, etc.), for a true demonstration of the potential for enhanced oil recovery, experiments in porous media must be performed. The experiments reported only consider flow of one phase (i.e., the water phase with or without polymer added), and the expected improvement in mobility ratio can be deduced from the mobility reduction (see Eq. 1), but the possible chemical influence of the presence of oil on the associative resistance to flow is not considered in this work. However, Lohne et al. [20], Reichenbach-Klinke, et al. [25] and Askarinezhad et al. [1] reported that the presence of oil did not significantly alter the improvement in mobility ratio.

As demonstrated by Leblanc et al. [18] and Reichenbach-Klinke et al. [26], a higher concentration is needed in bulk than in porous media to detect thermo-thickening, and in porous media the resistance to flow will be much higher than what one would expect from bulk viscosity measurements. Reichenbach-Klinke et al. [25]

reported resistance factor,  $RF$  matching the power law,  $RF = A\dot{\gamma}^{-\alpha} + RF_{\infty}$ , where  $\dot{\gamma}$  is the shear rate, for a range of TAPs.

Why the thickening effect of TAPs and hydrophobically associating polymers is enhanced in the porous media compared to in bulk is not fully understood. In bulk, Hourdet et al. [14] state that a critical concentration is needed for intermolecular association to dominate over intramolecular association. At low shear rates Zhong et al. [37] noticed that associative polymers can be shear-thickening. This is not in contradiction to the more commonly observed shear-thinning referred above; after the initial shear-thickening at low shear rates, these polymers also experienced shear-thinning.

Shear-thickening for associating polymers was also observed by Bokias et al. [3]. Both Zhong et al. [37] and Bokias et al. [3] attributed the shear-thickening to insufficient deformation at low shear rates favoring intramolecular associations whereas deformation as shear rate increases favors intermolecular associations, as was also noted by Seright et al. [28]. During porous media flow, the polymers will constantly change their conformation. This can possibly explain why the thickening of associative polymers is more effective in porous media compared to in bulk.

A delayed response in reaching steady state resistance factor in core floods for associative polymer is well documented (see e.g. [26]). The extent of delay before reaching stable resistance factor varies with polymer properties and conditions. A delay of around 10 pore volumes is not uncommon.

Seright et al. [28] attributed the delay to chromatographic separation of an associative enriched fraction of the polymer solution and Dupuis et al. [9] similarly attributed it to adsorption/retention of a minor fraction of the polymer solution. In addition, it is a feature of polymers, that when they are subjected to changes in confined space, reaching equilibrium will be a very slow process. Israelachvili [15] reports a typical increase in time to reach equilibrium by a factor of  $10^{10}$ .

The delay effect was successfully modelled by Lohne et al. [20] for a TAP described by Reichenbach-Klinke et al. [25], by dividing the polymer into two fractions, one behaving as a regular polymer and one small fraction behaving as a hydrophobic polymer. The model was also upscaled to a synthetic field case and demonstrated a substantial increase in oil recovery and injectivity efficiency by using a low concentration of associative polymers, compared to a higher concentration of a traditional polymer. This was attributed to low resistance to flow in the low temperature and high rate injection areas and high resistance in the low rate and high temperature area of the main parts of the reservoir. The efficiency was reported as

barrels of incremental oil per kg polymer injected and was reported to be 2.00 for 300 ppm TAP, 1.47 for 500 ppm TAP and 0.58 for 500 ppm regular polymer.

In this work we have studied how resistance to flow, time to reach steady state, and shear rate-effects were influenced by temperature gradient, type of porous media, associative content, polymer concentration, salinity, and up-scaling from 7 to 76 cm.

Due to their many favorable trades, thermo-thickening associative polymers should be ideal candidates for enhanced oil recovery, as they will have a low resistance to flow in the often cooled down, high rate injection area and high resistance to flow in the high temperature, low rate main part of the reservoir. Thus, a lower molecular weight polymer can be used, which has a smaller risk of mechanical degradation. They can presumably also be designed to fit reservoir conditions (temperature, temperature gradient, permeability, and salinity) by incorporating different thermosensitive polymers onto the main polymer.

## 2 Theory and definitions

In this work, we performed core floods and derived resistance factor for cores and capillary tubes from differential pressure readings. The role of polymer in enhanced oil recovery is to reduce the mobility ratio,  $M$ , defined as  $M = \lambda_{displacing} / \lambda_{displaced}$ , where  $\lambda$  is the mobility.

To quantify a polymeric solutions ability to reduce  $M$  in polymer core flood experiments, it is normal to report the resistance factor,  $RF$ , also commonly referred to as the mobility reduction, which is the ratio describing how much the mobility ratio,  $M$  is improved by polymer compared to water. From Darcy's law in cylindrical cores the porous media resistance factor,  $RF_{pm}$ , is given by:

$$RF_{pm} = \frac{\lambda_w}{\lambda_p} = \frac{\eta_p k_w}{\eta_w k_p} = \frac{\Delta P_p}{\Delta P_w} \quad (1)$$

where  $\eta$  is the viscosity,  $k$  is the permeability and  $\Delta P$  is the differential pressure. The subscripts,  $p$  and  $w$ , are for polymer solution and water, respectively.

Correspondingly, the resistance factor, mobility reduction in the capillary tubes,  $RF_{CT}$  is defined as:

$$RF_{CT} = \frac{\Delta P_p}{\Delta P_w} \quad (2)$$

Using the Hagen-Poiseuille equation for laminar Newtonian flow, and assuming it also holds for polymer solutions, the capillary tube resistance factor,  $RF_{CT}$ , is equal to the relative viscosity;

$$RF_{CT} = \frac{\Delta P_p}{\Delta P_w} = \frac{\eta_p}{\eta_w} = \eta_r \quad (3)$$

Then, a capillary tube can be used as an in-line viscometer, while the apparent viscosity ( $= RF_{pm}$ ) derived from a porous media, also contain the term  $\frac{k_w}{k_p}$ , known as the residual resistance factor,  $RRF$ . Retention of polymer because of adsorption, precipitation and gel formation are the main reasons why  $k_p < k_w$ .

The viscosity of polymer solutions is shear dependent and the viscosity of the solutions used in this work can be fitted to the Carreau model:

$$\eta(\dot{\gamma}) = \eta_w + (\eta_0 - \eta_w) \left[ 1 + (\lambda \dot{\gamma})^2 \right]^{\frac{n-1}{2}} \quad (4)$$

Here,  $\eta_0$  is the zero shear rate viscosity (also known as the Newtonian viscosity),  $\eta(\dot{\gamma})$  is the viscosity at the shear rate,  $\dot{\gamma}$ ,  $n$  is the power law index, and  $\lambda$  is the relaxation time which is essentially the invers of the shear rate at which a Carreau fluid becomes shear-thinning.

In capillary tubes for a Newtonian fluid, the shear rate at the wall,  $\dot{\gamma}_{ct}$  can be calculated from Hagen-Poiseuille equation. According to Sorbie [31], a correction factor,  $\frac{1+3n}{4n}$ , (where  $n$  is the power law index), must be applied for power law fluids. In this work, with values of  $n$  resulting in correction factors below 1.1, we neglect the correction factor when calculating the shear rate in capillary tubes and use the equation as presented:

$$\dot{\gamma}_{ct} = \frac{4\langle v \rangle}{R} = \frac{4Q}{\pi R^3} \quad (5)$$

Here,  $\langle v \rangle = Q/\pi R^2$  is the mean velocity and the shear rate is proportional to the flow velocity.

Equation 5 can also be the basis for calculating shear rate,  $\dot{\gamma}_{pm}$ , in a porous media with porosity  $\phi$ , by assuming that the porous media is a bundle of capillary tubes, so that  $R^2 = \frac{8k}{\phi}$ . This approach is analogue to Chauveteau and Sorbie [6], Cannella et al. [4], and Teeuw and Hesselink [35]. To account for the facts that the porous media is not a bundle of capillary tubes and that the polymeric solution has non-Newtonian flow behavior a correction factor,  $\alpha$  is introduced. In this work we used the correction factor,  $\alpha = 2.5$ , reported for sand packs by Chauveteau and Sorbie [6] and later used in works by e.g., Stavland et al. [33] and Reichenbach-Klinke et al. [25].

$$\dot{\gamma}_{pm} = \frac{4\alpha v}{\sqrt{8k/\phi}} = \frac{4\alpha Q}{\pi R^2 \sqrt{8k\phi}} \quad (6)$$

### 3 Materials and methods

The flow behavior of the polymer solutions was studied in cylindrical cores and sand packs. Two different brines were used to make the polymer solutions. The first brine, Synthetic Sea Water (SSW) had sea-water-like salinity, with 28 g/l NaCl and 8.0 g/l  $\text{CaCl}_2 \times 2\text{H}_2\text{O}$  as the salts. The high salinity brine (3xSSW), had 3 times the concentration of SSW, that is 84 g/l NaCl and 24 g/l  $\text{CaCl}_2 \times 2\text{H}_2\text{O}$ . Brines were filtered through a 0.45-micron Milipore filter before use.

The salinity effect on the viscosity in mixing brines is computed using molar weighted contributions from individual salts obtained from CRC's Handbook of Chemistry and Physics, 63rd edition [36]. The relative viscosity increase is computed at 20 °C and the temperature dependency is assumed to follow that of pure water. The calculated viscosity of SSW is 1.060, 0.494 and 0.375 cP, and 1.194, 0.556 and 0.423 cP for 3xSSW at 20 °C, 60 °C and 80 °C, respectively.

Before mixing in the polymer, all brines were purged with pure nitrogen (99.999%), as oxygen can induce chemical degradation of synthetic polymers [12, 29].

The thermo-thickening associative polymers tested in this work were obtained from BASF and are of the type described in Langlotz et al. [17]. Three different polymers were studied: A06, A08 and A10. The relative viscosity of the polymer solutions, as calculated from bulk rheology measurements at 20 °C (see Eq. 3) can be found in Fig. 9 and Fig. 10. The water-soluble main polymer was a 25 mol-% AMPS – acrylamide copolymer with a molecular weight of 5–8 million Dalton (AMPS = 2-Acrylamido-2-methylpropane sulfonic acid). The relative associative content differed and was 0.6 and 0.8, relative to A10 for A06 and A08, respectively.

The ready-to-use polymer solutions were prepared from pre-made 1 wt.% (10 000 ppm) stock solution. The stock-solutions were mixed by standard method, using a Heidolph RZR 2021 mixer. After mixing for 0.5 h at 300 rpm, the speed was lowered to 200 rpm, and mixing and hydration commenced overnight. During mixing, the solution was covered. During storage, the solutions were covered with a nitrogen blanket, capped, and kept in a refrigerator.

The diluted solutions were mixed just prior to use, on a magnet stirrer while purging with pure nitrogen. The diluted solution was stirred and purged for at least 0.5 h, before it was swiftly transferred to the pump-reservoir for immediate use. Foam was generated during purging and mixing. The viscosities of the polymer solutions were measured as a function of shear rate by a cone and plate geometry with an Anton Paar MCR301 Rheometer

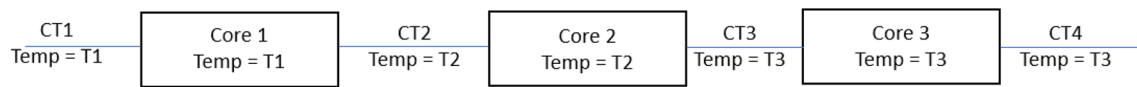


**Fig. 1** Sketch of the experimental set-up/flooding rig with 3 cores and capillary tubed in series. The injection direction is from left to right, from low to high temperature. T1 was 20 °C in all the experi-

ments. T2 was 60 °C and T3 was 80 °C, in all but the first experiment (Experiment 1a), where they were 30 °C and 60 °C, respectively

**Table 1** Overview of Experiment 1 to 6. The brine was synthetic sea water (SSW)

Exp	Polymer	Conc. ppm	Core type	T1 °C	T2 °C	T3 °C
1a	A06	1000	Bentheimer	20	30	60
1b	A06	1000	Bentheimer	20	60	80
2	A06	2700	Bentheimer	20	60	80
3	A08	1000	Bentheimer	20	60	80
4	A10	1000	Bentheimer	20	60	80
5	A10	1000	Sand	20	60	80
6	A10	1000	Berea	20	60	80

(at 20 °C). No prefiltering of the polymer solutions was performed, but the inlet core at 20 °C, where no thermo-thickening takes place, will act as a filter, rendering the results in the following cores unaffected by any lack of pre-filtering.

Two different flooding rigs were used. In the first (see Fig. 1), three cores of the same type of porous media were mounted in core holders with overburden pressure of 50 bar. For the unconsolidated sand, thin slices (~0.5 cm) of Bentheimer were mounted on each side of the sand packs and satisfactory packing of the dry sand was ensured by vibration.

Pore volume was measured, and we derived permeability from rate steps and measured base line pressure drops for the capillary tubes at 20 °C.

The core holders were coupled in series, each placed at a different temperature. Injection was performed from low to higher temperature to imitate the effect of a reservoir with a cooled down injection area.

Each core holder was connected to two differential pressure transmitters (one with a high resolution, and one with a broad range). The pressure transmitters were Fuji and

**Table 2** Overview of Experiment 7 to 9, conducted with a 76 cm long unconsolidated sand pack in steel tube

Exp	Polymer	Conc. ppm	Core	Brine	T °C
7	A10	1000	Sand	SSW	80
8	A10	1000	Sand	3xSSW	80
9	A10	1000	Sand	3xSSW	Temp-steps

Honeywell transmitters. The capillary tubes (see Fig. 1) had internal diameter of 1.01 mm and length of 1 m and were used to derive viscosity and polymer break through time. A back-pressure of 10 bar was applied. The cores were 7 cm long and had a diameter of 3.8 cm. In Experiment 1 to 4, Bentheimer cores with a permeability of approximately 2 Darcy were used as the porous media. The same cores were used in all four experiments and no cleaning was performed between experiments. In Experiment 5 unconsolidated sand cores with a permeability of 8 Darcy were used. And in Experiment 6, Berea cores of 0.7 Darcy were used. For an overview of Experiment 1 to 9 see Table 1, 2. For more details on core properties, see Table 3.

**Table 3** Length, diameter, pore volume, porosity, and absolute permeability of the cores used in Experiment 1 to 6

Core #	Bentheimer			Berea			Sand		
	1	2	3	1	2	3	1	2	3
Temperature, °C	20	60	80	20	60	80	20	60	80
Core length, cm	6.98	6.97	6.94	7.04	7.04	7.05	7.90	7.43	7.13
Diameter, cm	3.78	3.78	3.78	3.78	3.76	3.76	3.79	3.78	3.78
Pore volume, ml	16.13	16.22	16.17	17.85	17.99	17.67	26.97	24.85	24.73
Porosity	0.207	0.208	0.208	0.226	0.229	0.226	0.326	0.326	0.346
Permeability, Darcy	1.96	1.92	1.73	0.663	0.680	0.691	7.39	8.32	8.49
Experiment #	1b to 4			6			5		

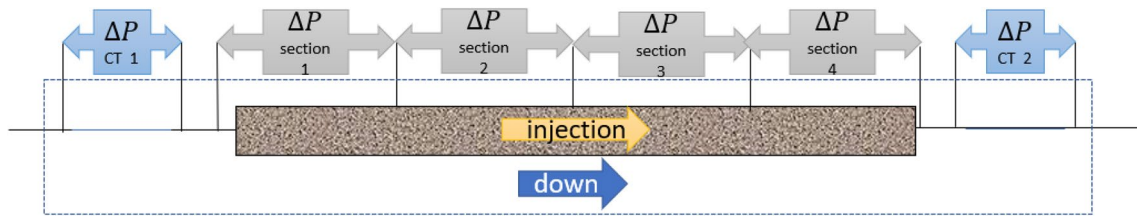


**Fig. 2** Sketch of the experimental set-up (flooding rig) with a 76 cm long sand pack in a steel cylinder used in Experiment 7 to 9. The dashed blue rectangle shows what is inside the heating cabinet. The blue lines show the capillary tubes (CT)

**Table 4** Length, diameter, pore volume, porosity, and absolute permeability, for each of the section and the entire pack, for the Sand pack used in Experiment 7 to 9

	Total	Section 1	Section 2	Section 3	Section 4
Length, cm	75.85	18.96	18.96	18.96	18.96
Diameter, cm	5.36	5.36	5.36	5.36	5.36
Pore volume, ml	592.34	148.09	148.09	148.09	148.09
Porosity	0.346	0.346	0.346	0.346	0.346
Absolute permeability, Darcy	11.78	11.37	13.20	11.65	11.04

Length, pore volume and porosity for each section were calculated from the total values

In the second set-up (see Fig. 2), a 76 cm long steel-cylinder with internal diameter of 5.36 cm was packed with the same type of unconsolidated sand, as used in Experiment 5. Satisfactory packing of the dry sand was ensured by vibration. Glass sinters were placed on each side of the sand pack. Pore volume and permeability were determined as for the first set-up.

Test conditions of the three experiments performed in the sand pack are shown in Table 2. The same sand pack was used in all three experiments and no cleaning was performed between experiments. The sand pack had a permeability of 12 D (for more details on sand properties see Table 4). The higher permeability compared to the sand pack in the core holders is due to the lack of overburden pressure in the steel cylinder. The cylinder was equipped with pressure ports enabling pressure drop readings over 4 equally spaced sections of the sand pack. As for the set-up with the core holder, two pressure transmitters were connected to each of the sections. The capillary tubes had the same dimensions as in the first set-up. The steel cylinder was mounted vertically in a heating cabinet with injection from the top. A back-pressure of 10 bar was applied.

The pump reservoir was equipped with a nitrogen blanket and a cap with a gasket for the tubing to the pump, ensuring an oxygen free environment. To avoid negative pressure, which may induce some noise in the pressure

readings, we made sure that the reservoir was not running low on polymer solution.

## 4 Results and discussion

### 4.1 Serial mounted cores

The purpose of Experiment 1 to 6 was to tune temperature and study the effect of temperature gradient, total polymer concentration and increasing associative content. When a system with satisfactory response was achieved, it was tested in both high permeable sand (Experiment 5) and Berea cores (Experiment 6), to investigate the effect of the nature of the porous media. The response ( $RF_{pm}$  and  $RF_{CT}$ ) is plotted as a function of pore volume (PV) injected, where pore volume injected is related to the pore volume of the first core. The properties of the cores and sand packs used in Experiment 1 to 6 are listed in Table 3. The stated properties of the sand are without considering the thin slices of Bentheimer at the inlet and outlet.

#### 4.1.1 Bentheimer cores

In experiment 1a, 74.3 PV of 1000 ppm A06 was injected at a volumetric flow rate,  $Q$  of 1 ml/min, then the flow rate was reduced to 0.2 ml/min. According to Eq. 5 and 6, the flow rate of 1 ml/min corresponds to shear rate of  $165 \text{ s}^{-1}$  in the capillary tubes and  $83\text{--}88 \text{ s}^{-1}$  in the Bentheimer cores. Differential pressure across cores and capillary tubes as a function of pore volumes injected are plotted in Fig. 3.

As expected, the differential pressure decreased with temperature and injection rate. To investigate if this is merely an effect of the viscosity's temperature dependence, the  $RF_{pm}$  and  $RF_{CT}$  (as calculated from Eq. 1 and 2) are plotted against pore volumes injected in Fig. 4.  $RF_{pm}$  at the same flow rate were essentially equal, and slightly higher than the  $RF_{CT}$ . This is consistent with the behavior anticipated for a regular polymer, where the higher resistance factor in the cores is caused by decreased polymer permeability ( $k_p < k_w$ , see Eq. 1) due to retention of polymer molecules. The increase in resistance factor when the

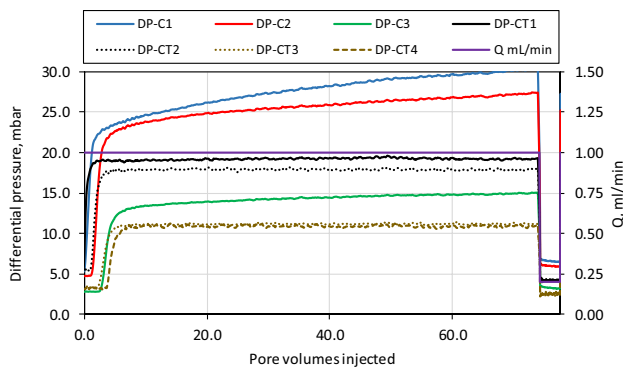


**Fig. 3** Experiment 1a. 1000 ppm A06 in SSW in Bentheimer. Differential pressure across cores and capillary tubes as a function of pore volumes injected in Core 1 (C1 at 20 °C), Core 2 (C2 at 30 °C), Core 3 (C3 at 60 °C). Number of pore volumes injected is calculated from the pore volume of Core 1

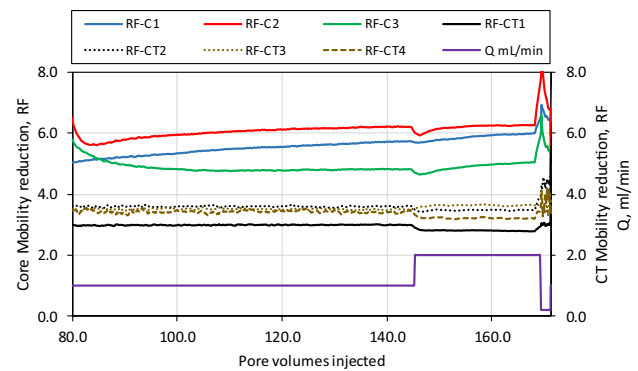


**Fig. 5** Experiment 1b. 1000 ppm A06 in SSW in Bentheimer. RF as a function of pore volumes injected in Cores and capillary tubes (CT). T1 = 20 °C, T2 = 60 °C and T3 = 80 °C. The volumetric injection rate is 1 ml/min for from 77.6 to 145 pore volume and 2 ml/min from 146 to 169 pore volumes and is thereafter decreased to 0.2 ml/min

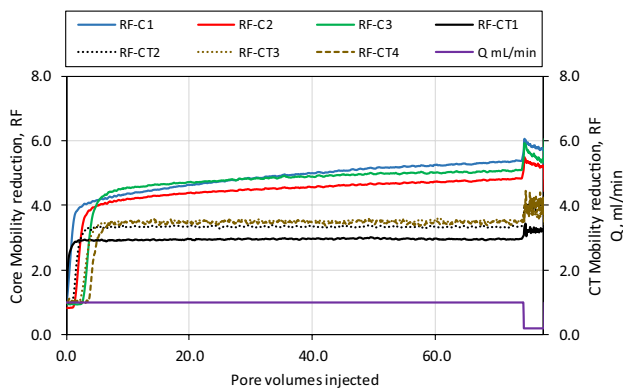


**Fig. 4** Experiment 1a. 1000 ppm A06 in SSW in Bentheimer.  $RF_{pm}$  as a function of pore volumes injected in Core 1 (C1 at 20 °C), Core 2 (C2 at 30 °C), Core 3 (C1 at 60 °C), and  $RF_{CT}$  for the capillary tube 1 (CT1 at 20 °C, upfront Core 1), capillary tube 2 (CT2 at 30 °C, upfront Core 2), capillary tube 3 (CT3 at 60 °C, upfront Core 3), and capillary tube 4 (CT4 also at 60 °C, but after Core 3). The volumetric injection rate is 1 ml/min for 74 pore volumes and is thereafter decreased to 0.2 ml/min for 3 additional pore volumes

rate was decreased is consistent with the shear-thinning behavior for regular polymer. It is thus concluded that no thermo-thickening was observed in experiment 1a.

Then, after injecting 77.6 PV of polymer solution, the temperatures were increased to 60 °C in Core 2, and to 80 °C in Core 3, for experiment 1b. As seen in Fig. 5, the 1000 ppm A06 polymer diluted in SSW did not yield thermo-thickening, even at 80 °C.

For Experiment 2, the concentration of the A06 polymer was increased from 1000 to 2700 ppm. The dilution brine, temperatures and cores were the same as in the previous experiment (1b) and the response (see Fig. 6) is plotted as a function of the cumulative volume of 2700 ppm polymer solution injected. The injection rate was 1.0 ml/min for 81

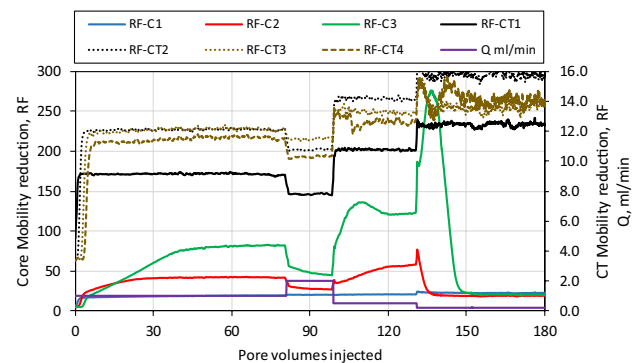


**Fig. 6** Experiment 2, 2700 ppm A06 in SSW in Bentheimer. RF as a function of pore volumes injected in Cores and capillary tubes (CT). T1 = 20 °C, T2 = 60 °C and T3 = 80 °C. The volumetric injection rate is 1 ml/min from 0 to 81 pore volume, 2 ml/min from 81 to 99 pore volumes, 0.5 ml/min from 99–131 PV and is thereafter decreased to 0.2 ml/min from 131–189 pore volumes

pore volumes, 2.0 ml/min for the next 18 PV, 0.5 for the next 32 PV and 0.2 ml/min for the last 58 PV.

The 2700 ppm A06 solution in SSW clearly demonstrated thermo-thickening in the porous media at 60 °C and 80 °C, while no thermo-thickening was observed at 20 °C. At 1 ml/min,  $RF_{pm}$  reached 82 in the core at 80 °C and 42 in the core at 60 °C. Doubling the flow rate, resulted in a reduction of the  $RF_{pm}$  by almost a factor 2, to  $RF_{pm} = 45$  at 80° and  $RF_{pm} = 27$  at 60 °C. A similar trend was observed when the rate was reduced to 0.5 ml/min, resulting in  $RF_{pm}$  of 122 and 57 for 80 °C and 60°, respectively. This agrees with observations made by Reichenbach-Klinke et al. [25], who reported a nearly constant differential pressure for flow rates varying two orders of magnitude for a similar TAP (with higher molecular weight and associative content at lower concentration). Further, it is worth mentioning

that due to the delayed effect, discussed below, stable condition may not have been reached at 2 ml/min.

Figure 6 also reveals thermo-thickening in the capillary tubes at 60 °C and 80 °C. Thus, the concentration of 2700 ppm was above the concentration at which this polymer demonstrates bulk thermo-thickening. However, the effect was significantly lower than the one observed in the cores.

A delay in reaching steady state resistance factors of approximately 20 PV and 39 PV for Core 2 and Core 3, respectively was observed at the initial injection rate. In contradiction to what is usually observed for more diluted solutions, the  $RF_{pm}$  started to increase in Core 3 before it reached steady state in Core 2, indicating that a fraction of the polymer, not sufficiently associating to thermo-thicken at 60 °C, moved through Core 2 at the velocity of the polymer front, and thermo-thickened at 80 °C.

After injecting 131 PV, the injection rate was lowered from 0.5 ml/min to 0.2 ml/min. The initial response was an increase in the  $RF_{pm}$  both in Core 2 and Core 3, shortly followed by a gradual decline in Core 2, which after approximately 5 PV was at the level expected for a regular polymer. The decline in Core 2 was accompanied by an increase in Core 3, reaching its transient maximum just as Core 2 reached regular polymer behavior. This could be explained by release from Core 2 of an associative-rich fraction, which is in a state where it is not sufficiently associative to form resistance to flow at 60 °C, but is at 80 °C. The state will then be the released fraction's conformation, hydrophobic content, strength of hydrophobic interaction or combination of these. The development of the  $RF_{pm}$  in Core 3 was even more intriguing. First, there was a build-up to the transient maximum followed by a decline. After the decline period of approximately 10 PV the  $RF_{pm}$  approached the level expected regular polymer. It is also interesting to see that the breakdown of the associative resistance to flow was accompanied by fluctuations in the CT3 and CT4 resistance factors (the CT before and after Core 3 at 80 °C). Both CT3 and CT4 declined as the resistance to flow broke down in Core 2, while CT4 increased again as resistance broke down in Core 3. The transient maximum in  $RF_{pm}$  for Core 3 at 0.5 ml/min was also accompanied by a minimum  $RF_{CT}$  in CT4. To sum up: The thermo-thickening increased with decreasing shear rate, up until a very low shear rate where the associative resistance to flow, after a transient increase, broke down and the polymer solution behaved as a regular polymer. This can be explained by the formation of intramolecular association which is not sufficiently disturbed at low shear rates to form new intermolecular association thus terminating the gel-like flow behavior.

In experiment 3 we tested if a polymer with a higher associative content could give a more robust

thermo-thickening response in the Bentheimer cores. A concentration of 1000 ppm of A08 in SSW was used as the polymer solution. Figure 7 shows the evolution in  $RF_{pm}$  as a function of pore volumes of A08-solution injected. The injection rate was 1.0 ml/min for the first 122 PV. Thereafter the flow rates were varied as depicted in Fig. 7.

Overall, the response in the cores was very similar to the response observed for 2700 ppm A06 in experiment 2. Thermo-thickening was achieved at 60 °C and 80 °C, the effect was significantly delayed in terms of volume needed, the resistance factor,  $RF_{pm}$  increased with decreasing shear rate, and at very low shear rate, breakdown of the associative resistance to flow occurred.

In this experiment  $RF_{pm}$  at 60 °C was somewhat higher than with 2700 ppm A06 at 60 °C, and at 80 °C it was the opposite; the  $RF_{pm}$  was higher for 2700 ppm A06. The slope in the decline in  $RF_2$  and  $RF_3$  during breakdown is less steep in this A08 experiment than in the 2700 A06 experiment, indicating that 1000 ppm A08 is more robust than 2700 ppm A06.

In terms of the delay, the number of pore volumes needed to reach stable resistance factor at the initial injection rate were approximately 43 PV and 92 PV for Core 2 and Core 3, respectively, twice the delay of experiment 2 which has twice the concentration of associative content (polymer concentration x associative content).

We also noted that Core 1 did not cause a delay in Core 2, strongly indicating that the mechanism that links the behavior of Core 2 and Core 3, is not at play when the polymer is in its purely hydrophilic state. This may seem obvious, but will be important for field implementation, where a delay caused by the areas with no effect would increase the time and volume needed for a response.

In experiment 4 we tested if a polymer with an even higher associative content could give a more robust

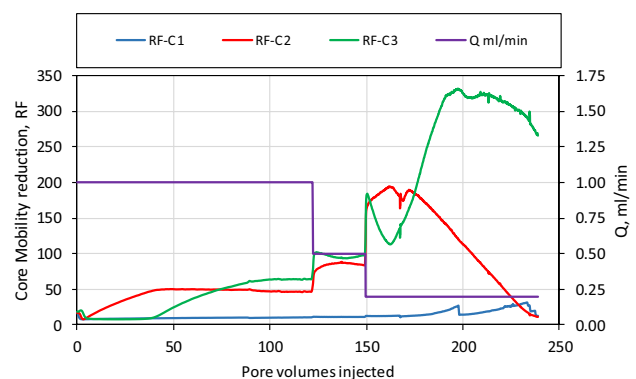


**Fig. 7** Experiment 3, 1000 ppm A08 in SSW in Bentheimer.  $RF_{pm}$  as a function of pore volumes injected.  $T_1=20$  °C,  $T_2=60$  °C and  $T_3=80$  °C. The volumetric injection rate is 1 ml/min ( $\dot{\gamma}_{pm} \sim 85s^{-1}$ ,  $\dot{\gamma}_{ct} = 165s^{-1}$ ) from 0 to 122 pore volume, 0.5 ml/min from 122–150 PV and 0.2 ml/min from 150–239 pore volumes



thermo-thickening response in the Bentheimer cores. A concentration of 1000 ppm of A10 in SSW was used as the polymer solution. Figure 8 shows the evolution in  $RF_{pm}$  as a function of pore volumes of A10-solution injected.

Overall, the response was faster (fewer pore volumes to reach plateau) and  $RF_{pm}$  higher than with the A08 polymer. A delay in reaching steady state resistance factors of approximately 15 PV and 26 PV for Core 2 and Core 3, respectively was observed at the initial injection rate. This is a much faster response then for the A08 with lower associative content with a delay of 43 PV and 92 PV, but the lack of cleaning between the experiments, makes it difficult to quantify the effect.

As mentioned above, the cores where not cleaned before changing polymer solution. Consequently, polymer solution from the previous experiment was still present in the cores at start of the injection This is probably the reason why  $RF$  in Core 3 was not equal to  $RF$  in Core 1 during the first 15 PV. Like the previous experiments, the resistance factor increased with decreasing shear rate. The previously observed breakdown of the associative network at the lowest shear rate, was, within the time of the experiment, only observed at 60 °C, but assuming a breakdown would follow the same trend as in experiment 3, probably at least 35 more pore volume should have been injected, that is, injection should have continued for 2 more days, to conclude that the resistance factor was truly stable at 80 °C.

The results from the Bentheimer experiments can be summed up by plotting the resistance factors in the cores and in the capillary tubes as a function of shear rate.

Figure 9 shows the resistance factor in the cores and capillary tubes for experiment 1b, 1000 ppm A06 in SSW revealing no thermo-thickening for this system for temperatures up to 80 °C. The  $RF_{CT}$  were practically equal to the

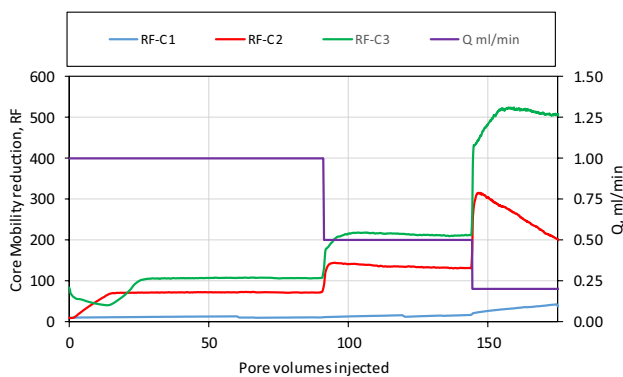


**Fig. 8** Experiment 4, 1000 ppm A10 in SSW in Bentheimer.  $RF_{pm}$  as a function of pore volumes injected.  $T_1=20$  °C,  $T_2=60$  °C and  $T_3=80$  °C. The volumetric injection rate is 1 ml/min from 0 to 91 pore volumes, and 0.5 ml/min from 91–147 PV and 0.2 ml/min from 147–176 pore volumes

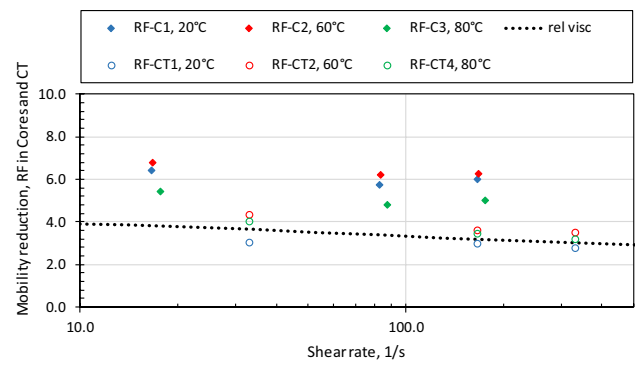


**Fig. 9** Experiment 1b.  $RF_{pm}$  and  $RF_{CT}$  and as a function of shear rate in the Bentheimer cores and capillary tubes (CT) for 1000 ppm A06 in SSW. Blue markers are used for 20 °C, red for 60 °C and green for 80 °C. The markers for the cores are filled diamonds and the markers for the capillary tubes are open circles. The dashed line shows the relative viscosity of 1000 ppm A06 in SSW from the Carreau model (Eq. 4) fitted to measurements performed with Anton Paar Rheometer at 20 °C

relative viscosity, demonstrating the validity of using the capillary tubes as in-line viscometers for tracking potential degradation and breakthrough of polymer solution from the cores.

For Experiment 2 to 4, where thermo-thickening was observed, the resistance factor in the cores and in the capillaries are plotted in two different figures. Figure 10 show the results for the cores. The measured values after breakdown of the resistance to flow at the lowest shear rates are plotted as larger open symbols. The dashed lines show the Carreau modeled relative viscosities of the 3 polymer

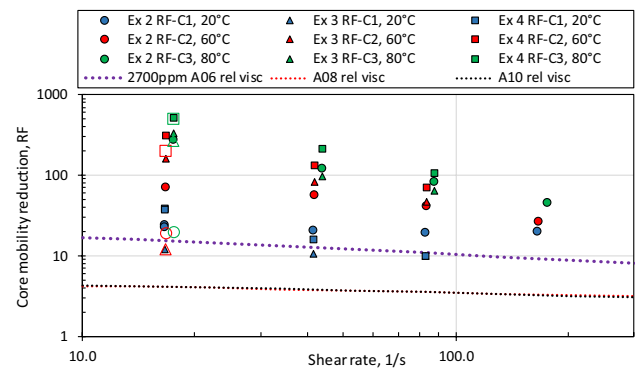


**Fig. 10**  $RF_{pm}$  as a function of shear rate in the Bentheimer cores in Experiment 2 – 2700 ppm A06, Experiment 3 – 1000 ppm A08 and Experiment 4 – 1000 ppm A10, all in SSW. Both the maximum  $RF_{pm}$  (filled symbols), and  $RF_{pm}$  after breakdown (open symbols) are plotted. The squares are used for Experiments 4, triangles for Experiment 3 and circles for Experiment 2. Blue markers are used for 20 °C, red for 60 °C and green for 80 °C. The dashed lines are the relative viscosities from the Carreau model (Eq. 4) fitted to measurements performed with Anton Paar Rheometer at 20 °C

solutions. The magnitude of the mobility reduction with 1000 ppm A10 and A08 are virtually equal.

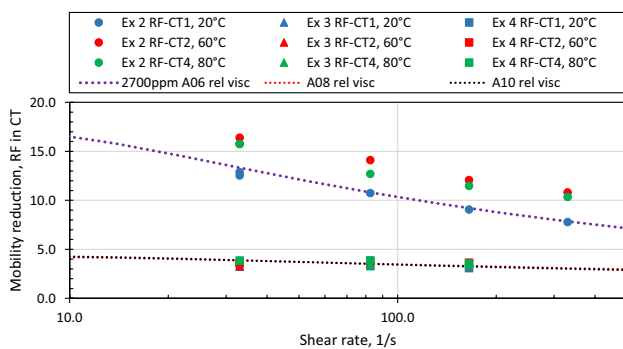
Thermo-thickening in the cores was observed with all 3 polymer solutions at 60 °C and 80 °C. Resistance factors up-to 100 times higher than expected for a regular polymer were measured. The thermo-thickening resistance factor's shear dependence was also evident.

Figure 11 compares the relative viscosities of the 3 different polymer solutions to the resistance factor measured in the capillary tubes in Experiment 2, 3 and 4. For the 1000 ppm solutions at all temperatures and the 2700 ppm at 20 °C, the  $RF_{CT}$  were as expected from viscosity measurements performed with the Anton Paar Rheometer. At 60 °C and 80 °C the 2700 ppm solution displayed signs of thermo-thickening in the capillary, which is consistent with statements that a high concentration of TAPs is needed to observe thermo-thickening in bulk.

After having injected over 12 L (780 PV) of polymer solution, we started injecting brine at 1 ml/min. After injecting ~ 450 PV of brine, the residual resistance factor (RRF) was 2.4 in Core 2 and 1.9 in Core 3 (and still declining). In Core 1, where a slight increase in resistance to flow was already seen during the last part of the polymer injection, the resistance to flow increased dramatically to an RRF of around 50. This can perhaps be partly explained by the large throughput of polymer during the test.

### 4.1.2 High permeable unconsolidated sand

Experiment 5 was performed with the same polymer solution as Experiment 4, 1000 ppm A10 in SSW, to investigate the porous media's influence on the system's ability to thermo-thicken. Except for the porous media, the test



**Fig. 11**  $RF_{CT}$  as a function of shear rate in the Capillary tubes (CT) in Experiment 2 – 2700 ppm A06, Experiment 3 – 1000 ppm A08 and Experiment 4 – 1000 ppm A10, all in SSW. The squares are used for Experiments 4, triangles for Experiment 3 and circles for Experiment 2. Blue markers are used for 20 °C, red for 60 °C and green for 80 °C. The dashed lines are the relative viscosities from the Carreau model (Eq. 4.) fitted to measurements performed with Anton Paar Rheometer at 20 °C

conditions were the same. The resistance factors in the cores as a function of pore volumes injected are plotted and depicted in Fig. 12. The injection rate was 1.0 ml/min ( $\dot{\gamma}_{pm} \sim 40s^{-1}$ ,  $\dot{\gamma}_{ct} = 165s^{-1}$ ) for the first 83 PV. Thereafter the flow rates were varied as shown in Fig. 12.

The lower  $RF_{pm}$  at 80 °C than at 60 °C for the first two injection rates, is presumably because the volume injected was too small to reach a plateau. This claim is supported by the slow build-up in Core 3 at 0.2 ml/min, and the higher resistance factor reached during the second (compared to the first time) injecting at 0.5 ml/min in the third core, where it reached over 400 and was still increasing when polymer injection was terminated.

The behavior in the sand cores was similar to the behavior of the same polymer solution in Bentheimer in that, at the initial rate, the increase in  $RF_{pm}$  in Core 3 started as it reached steady state in Core 2, and that, at the lowest rate,  $RF_{pm}$  broke down in Core 2. Increasing the rate demonstrated that the breakdown was reversible. The longer delay in the sand then in Bentheimer in reaching stable  $RF_{pm}$  is more likely to be an effect of starting with clean sand, possibly combined with the lower shear rate, rather than an effect of different porous media. The higher  $RF_{pm}$  at 60 °C, is mainly an effect of lower shear rate in the sand than in the Bentheimer, as will be demonstrated later.

### 4.1.3 Berea

Experiment 6 was performed with the same polymer solution (1000 ppm A10 in SSW) as Experiment 4 and Experiment 5, (made from a new batch of polymer powder). Except for the porous media the test conditions were the same. The resistance factors for the cores as a function of pore volumes injected are plotted in Fig. 13. The injection

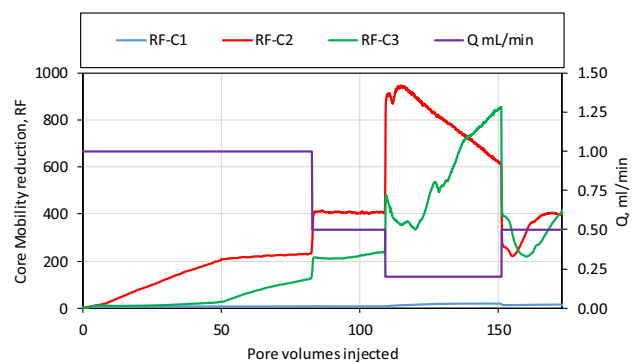


**Fig. 12** Experiment 5, 1000 ppm A10 in SSW in unconsolidated sand cores.  $RF_{pm}$  as a function of pore volumes injected. T1 = 20 °C, T2 = 60 °C and T3 = 80 °C. The volumetric injection rate is 1 ml/min ( $\dot{\gamma}_{pm} \sim 40s^{-1}$ ,  $\dot{\gamma}_{ct} = 165s^{-1}$ ) from 0 to 83 pore volumes, and 0.5 ml/min from 83–109 pore volumes, 0.2 ml/min from 109–154 pore volumes and 0.5 ml/min from 151–173 pore volumes

rate was 0.5 ml/min ( $\dot{\gamma}_{pm} \sim 67s^{-1}$ ,  $\dot{\gamma}_{ct} = 82.5s^{-1}$ ) for the first 128 PV. Thereafter the flow rates were varied as shown in Fig. 13.

In contrast to what was observed in sand and Bentheimer, the build-up of the resistance factor in the Berea cores happened in Core 2 at 60 °C after it increased in Core 3 at 80 °C and was lower at 80 °C than at 60 °C. Whether this is a measuring artifact, a consequence of a new polymer batch or representative for this polymer in Berea, is not yet fully understood.

#### 4.1.4 Comparing Berea, sand and Bentheimer

As discussed above, the resistance to flow of TAPs is strongly shear-thinning. To compare the results in the different porous medias it is thus appropriate to present the  $RF_{pm}$  as a function of shear rate in the porous media. Figure 14 shows the resistance factor as a function of shear rate for 1000 ppm A10 polymer solution in three different porous media at 20 °C, 60 °C and 80 °C. The dashed lines are  $RF = A\dot{\gamma}^{-\alpha} + RF_{\infty}$ , with  $A=11$ ,  $\alpha=0.1$  and  $RF_{\infty}=1$  for the blue line representing the trend at 20 °C and with  $A=3800$ ,  $\alpha=0.9$  and  $RF_{\infty}=1$  for the red line, representing the trend at 60 °C.

Disregarding 20 °C in Experiment 4 (due to high through-put) and the two lowest shear rates at 80 °C in Experiment 6 (because steady state presumably not reached), plotting  $RF_{pm}$  as a function of shear rate reveals that this polymer solution was thermo-thickening at 60 °C and 80 °C, but not at 20 °C. It is also shown that in term of  $RF_{pm}$  vs. shear rate, the behavior in the different porous media was equal. Also, increasing the temperature from 60 °C to 80 °C had little effect on the magnitude of  $RF_{pm}$ ,

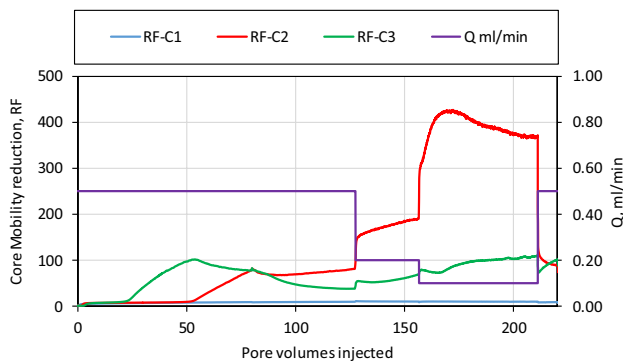


**Fig. 13** Experiment 6, 1000 ppm A10 in SSW in Berea cores.  $RF_{pm}$  as a function of pore volumes injected.  $T_1=20$  °C,  $T_2=60$  °C and  $T_3=80$  °C. The volumetric injection rate is 0.5 ml/min ( $\dot{\gamma}_{pm} \sim 67s^{-1}$ ,  $\dot{\gamma}_{ct} = 82.5s^{-1}$ ) from 0 to 127.5 pore volumes, and 0.2 ml/min from 127.5–157 pore volumes, 0.1 ml/min from 157–211 pore volumes and 0.5 ml/min from 211–220 pore volumes

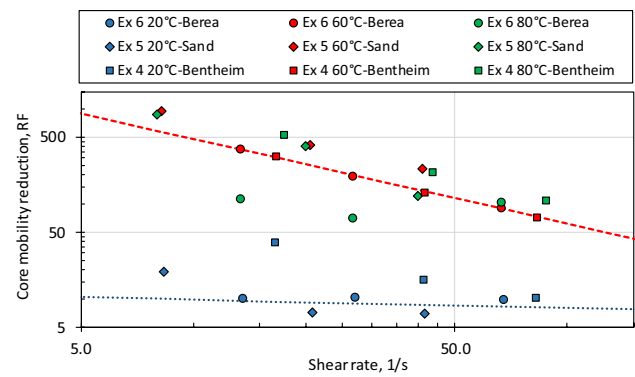


**Fig. 14**  $RF_{pm}$  with 1000 ppm A10 in SSW as a function of shear rate in the Bentheimer cores in Experiment 4, Sand cores in Experiment 5 and Berea cores in Experiment 6. Only the maximum  $RF_{pm}$  are plotted. The squares are used for Experiment 4, diamonds for Experiment 5 and circles for Experiment 6. Blue markers are used for 20 °C, red for 60 °C and green for 80 °C. The dashed red line represents the trend at 60 °C and the dashed blue line represents the trend at 20 °C. Note that the y-axis is from 5 to 1500 and the x-axis is from 5 to 150  $s^{-1}$

but as indicated earlier, the temperature may have an impact of the resistance to breakdown at low shear rates.

#### 4.2 Sand pack in steel cylinder with pressure ports

Experiment 7 was performed with the same polymer solution (1000 ppm A10 in SSW) as in Experiment 4 to 6. The objective was to investigate whether core length had any impact on the thermo-thickening. The temperature was 80 °C and the properties of the unconsolidated sand are listed in Table 4.

Figure 15 shows the resistance factors, in each of the four sections and in the capillary tubes, as a function of pore volumes injected (calculated from the pore volume of

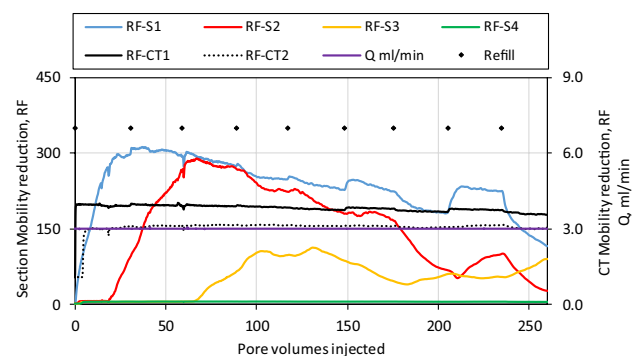


**Fig. 15** Experiment 7, 1000 ppm A10 in SSW in Sand column.  $RF_{pm}$  and  $RF_{CT}$  as a function of pore volumes injected in the sections.  $T=80$  °C. The volumetric injection rate is 3.0 ml/min ( $\dot{\gamma}_{pm} \sim 40s^{-1}$ ,  $\dot{\gamma}_{ct} = 495s^{-1}$ ) from 0 to 262 pore volumes. The black dots indicate when the polymer solution reservoir was refilled

one section = 148.09 ml). The injection rate was 3.0 ml/min ( $\dot{\gamma}_{pm} \sim 40s^{-1}$ ,  $\dot{\gamma}_{ct} = 495s^{-1}$ ) for the duration of the experiment, from 0–262 pore volumes.

In the first section, thermo-thickening began immediately and started leveling off after injection of 19 PV, immediately followed by onset of thermo-thickening in Sect. 2. Onset of thermo-thickening in Sect. 3 started at 65 PV. Within the time frame of this experiment, no thermo-thickening was observed in the fourth section. In Sect. 1,  $RF_{pm}$  peaked at 300, which is comparable in magnitude with the results shown in Fig. 14.

The  $RF_{CT}$  in the front capillary tube (CT1) was slightly higher than the effluent  $RF_{CT}$  (CT2). One may see this as an indication of degradation but comparing the  $RF_{CT}$  in the capillary tubes to the relative viscosity of the polymer solution at  $495 s^{-1}$  reveals that it is the resistance factor in CT1 that is higher than expected and not  $RF_{CT2}$  that is lower. The difference in capillary tube resistance factors may therefore be an indication of bulk thermo-thickening at inlet (CT1) and not at outlet (CT2). This interpretation is supported by the lack of thermo-thickening in Sect. 4 (and will be further supported by observations made in the next experiment).

The black dots in Fig. 15 indicate when the reservoir was refilled with fresh polymer solution. The viscosity of the different solutions varied, the Newtonian viscosity at 20 °C was  $5.04 \pm 0.25$  cP and this viscosity variation can explain some of the fluctuations in resistance factor with pore volume. However, the resistance factor in both Sect. 1 and 2 declined by volume injected. At the same shear rate in the 7-cm long sand pack, ( $q = 1.0$  ml/min in Experiment 5) no decline was observed.

Since no thermo-thickening was detected in Sect. 4 after injecting 262 PV (for close to 9 days), we increased the salinity 3 times (3xSSW) for Experiment 8. The polymer concentration was kept fixed at 1000 ppm of A10. The motivation was to achieve a more pronounced thermo-thickening effect induced by higher salinity. The temperature was maintained at 80 °C. The  $RF_{pm}$  in each of the four sections and  $RF_{CT}$  in the capillary tubes, as a function of pore volumes injected are plotted in Fig. 16. For the first 199 PV, the injection rate was 3.0 ml/min.

The increased salinity triggered thermo-thickening in all four sections. As expected, the increased salinity resulted in higher  $RF_{pm}$  (approximately 800 compared to 300 in the SSW case). The response also seems to be faster. Thus, in addition to temperature and polymer properties, the salinity can also be used to tune thermo-thickening. Figure 16 shows that the  $RF_{CT}$  in the second capillary tube (CT2) increased and approached  $RF_{CT}$  (CT1). This can be interpreted as thermo-thickening in the effluent capillary tube, substantiating the claim that the lower effluent resistance factor compared to the injected in Experiment

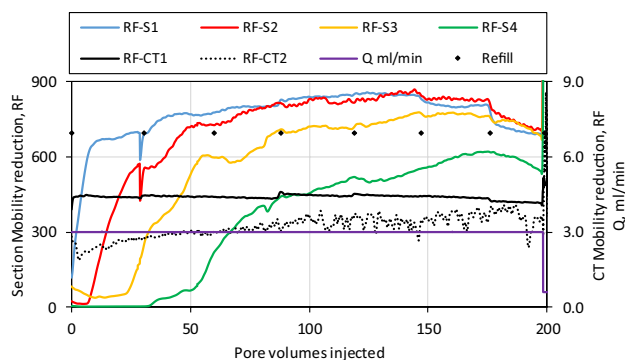


**Fig. 16** Experiment 8, 1000 ppm A10 in 3xSSW in Sand column.  $RF_{pm}$  and  $RF_{CT}$  as a function of pore volumes injected.  $T = 80$  °C. The volumetric injection rate is 3.0 ml/min from 0 to 198 pore volumes. The black dots indicate when the polymer solution reservoir was refilled

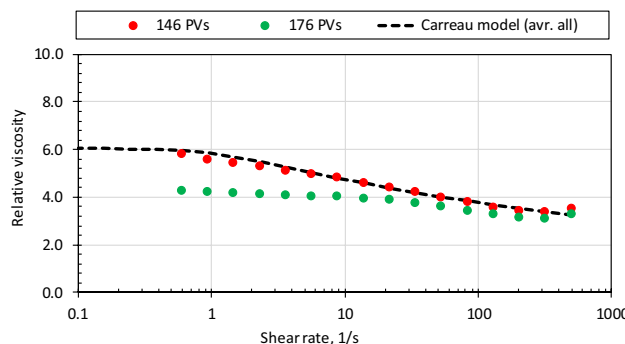


**Fig. 17** Relative viscosity as a function of shear rate for 1000 ppm A10 in 3xSSW for the sample refilled at 146 PV and 176 PV in Experiment 8. The dashed line represents the Carreau model for the average of all 1000 ppm A10 in 3xSSW samples mixed

7 (see Fig. 15) was due to lack of thermo-thickening, rather than degradation.

As for the previous experiments, the viscosity of the different mixes of polymer solution varied. The dip in section resistance factors, accompanying the refill at 176 PV in Fig. 16, is probably linked to the lower viscosity of this sample of polymer solution. Figure 17 shows the relative viscosity as a function of shear rate for the polymer mixes refilled at 146 and 176 PV, and the Carreau model (see Eq. 4) fitted to the average measurements for all the mixed solutions.

An alternative presentation of the results that are shown in Fig. 15 and Fig. 16, is to plot the cumulative resistance factors as a function of the corresponding pore volume, i.e., the resistance factors,  $RF_{pm}$  reported in Fig. 18 and Fig. 19 are across the first  $\frac{1}{4}$ ,  $\frac{1}{2}$ ,  $\frac{3}{4}$  and the entire sand column. As seen in Fig. 18, the  $RF_{pm}$  declined with increasing core length, while Fig. 19, for the 3xSSW case, shows

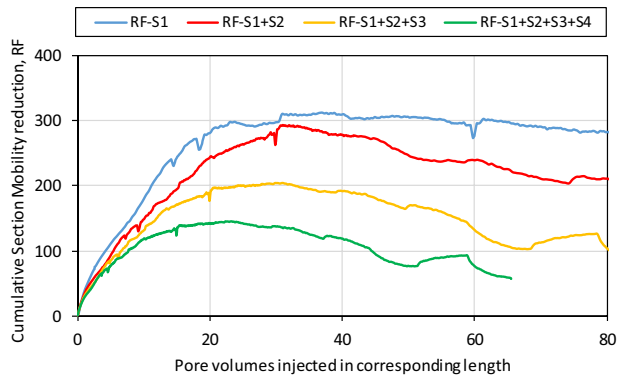


**Fig. 18** Experiment 7, 1000 ppm A10 in SSW in 76 cm sand column. Cumulative  $RF_{pm}$  as a function of pore volume cumulated over the corresponding length. The volumetric injection rate is 3.0 ml/min

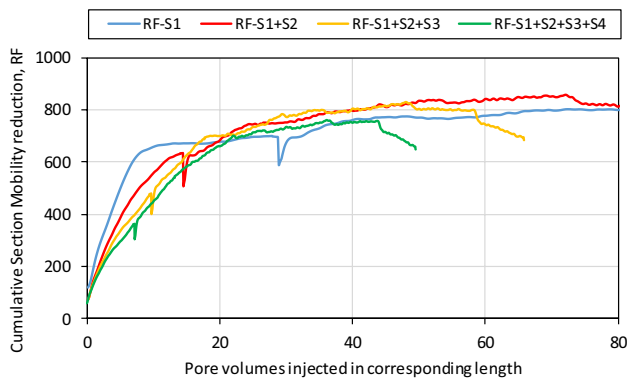


**Fig. 19** Experiment 8, 1000 ppm A10 in 3xSSW in 76 cm sand column. Cumulative  $RF_{pm}$  as a function of pore volume cumulated over the corresponding length. The volumetric injection rate is 3.0 ml/min

that the resistance factors nearly overlap. Thus, making the 1000 ppm A10 polymer more robust (here by increasing the salinity) nearly eliminated the length effect. This addresses the importance of applying a robust polymer design when upscaled to in-depth thermo-thickening at field conditions.

Finally, in Experiment 9, we varied the temperature during injection of the 1000 ppm A10 in 3xSSW. The flow rate was 0.6 ml/min ( $\dot{\gamma}_{pm} \sim 8s^{-1}$ ). The temperature steps are shown in Fig. 20. Firstly, we confirmed that  $RF_{pm}$  increased by decreasing the shear rate. At shear rate of  $8s^{-1}$ , the resistance factor in the 4 segments increased to 2500. At 60 °C, the resistance factor dropped to approximately 2000. Note that the initial decline in  $RF$ , which can be interpreted as a response to altering the steady state conditions, was followed by a build-up. As for the previous experiments, the build-up in one of the sections did not start before the subsequent section has reached steady

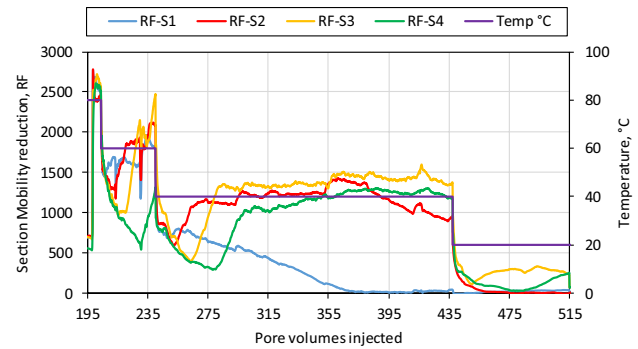


**Fig. 20** Experiment 9, temperature steps, 1000 ppm A10 in 3xSSW.  $RF_{pm}$  as a function of pore volumes injected. Volumetric injection rate is 0.6 ml/min from 198.2 PV.  $T=80^{\circ}$  to 203.9 PV.  $T=60^{\circ}$  C from 203.9 to 240.1 PV,  $T=40^{\circ}$  C from 240.1 to 437.6 PV, where up on temperature was lowered to 20 °C

state. A somewhat similar trend was observed when the temperature was reduced to 40 °C. In the first section,  $RF_{pm}$  steadily declined, while in the other sections,  $RF_{pm}$  approached 1200. As  $RF_{pm}$  in Sect. 1 reached  $RF_{pm}$  expected for a regular polymer solution, a similar decline of  $RF_{pm}$  began in Sect. 2. Thus, if larger volumes had been injected one may expect decline also in Sects. 2 to 4. The interpretation is, that for this system, the critical temperature for onset of thermo-thickening is above and close to 40 °C. When the temperature was lowered to 20 °C, the resistance factor in Sects. 2 to 3 dropped significantly. However, to reach steady state required large volumes.

During subsequent brine injection,  $RRF$  decline slowly. After injecting nearly 300 PV of 3xSSW brine,  $RRF$  was 5.7, 4.7 and 10.1 in Sects. 2, 3 and 4, respectively.

## 5 Concluding remarks

When discussing the nature of and the reason for the slow reaction to changes in condition of the TAP system, there are several considerations one should keep in mind.

The polymer molecules are not equal, that is, they are not of the same molecular weight. The molecular weight is distributed around the weight average molecular weight, usually with a tail at high molecular weight. Since they are randomly co-polymerized, they will neither have the same content of the thermo-sensitive polymer. This could mean that only a fraction of the molecules has the attributes needed to form the associative resistance to flow, and a certain amount of this fraction must be injected before steady state is reached. From the strong coupling of the behavior of neighboring cores/sections it seems that all of or close to all of this fraction is consumed during build-up off the associative network/gel. From the viscosity in the capillary tubes, which is not delayed, it does not seem

likely that the attribute is linked to the molecular weight of the polymer.

A well-known feature of polymers in confined spaces is the long time it takes to reach equilibrium, compared to the time it takes when space is not limited, inducing time-, history- and hysteresis-effects in these situations [15]. In the porous media with on-going flow, the space available to the individual polymers is restricted and constantly changing, narrowing, and expanding, which does not only change the space available, but also the forces exerted on the polymer molecules by the flow field. The time to reach steady state, whether it is as a response to flow rate, temperature or injected fluid will depend on several factors, all which will be influenced by changes in external conditions and need time to reach steady state. We therefore expect that the following factors will be important:

- The balance between adsorption and desorption.
- The conformation of the adsorbed molecules, which may change with time from a weakly adsorbed coil to a flat structure with more anchoring points [15].
- The adsorbed molecules' ability to associate with molecules in the solution.
- The relative amount of the different conformation of polymer molecules in solution (stretched, coiled, associated), and the different conformations activity towards adsorption and association.
- The nature and strength of the association: Are the polymer molecules associated with themselves (intramolecular association) or with one, a few or several other polymer molecules?
- The strength of the association compared to the external forces applied by the flow.

Regarding the enhanced thickening effect in porous media compared to in bulk, we see 3 possible, maybe not mutual exclusive, explanations. It could be due to adsorption of polymer molecules acting as anchoring points for the associative gel. It could be because the associative gel is continuous in the pore network and has to be strongly deformed or disrupted to move (or maybe it does not move at all, but fresh polymer molecules have to move through the gel-network constituting a secondary porous media, by reptation). Or it could be because in porous media flow, the conformation of the polymer molecules is changing and extended, exposing the associative groups (hydrophobic stickers) to part-take in intermolecular association as opposed to intra-molecular association. This will lead to a dynamic associative network, where association is continuously being formed and disrupted so that new associative binding can be formed. The associating groups can be seen as weak sticker on ropes being pulled over each other in different directions, when one sticker

is forced out of contact with another sticker, it will stick to the next it comes in contact with. The strongly shear-thinning nature of the resistance factor is then caused by the ease of breaking the intermolecular association at high flow rates, and the breakdown of resistance to flow at very low shear rates would be due to the formation of intramolecular association when the polymer molecule coils up on themselves.

The large volumes need of the tested polymer solutions to reach steady state, represents a considerable challenge with regards to field implementation for traditional EOR-purposes. Understanding the polymer-polymer and polymer-porous media interactions will provide valuable information when attempting to design a thermo-thickening polymer system more suitable for this purpose. Future pore net-work modelling, as described for complex fluids by for instance Didari et al. [8] and Lopez et al. [21] and pore scale molecular dynamics simulations of polymer chains in confined spaces as described by Palmer et al. [24] may reveal valuable information in this regard.

## 6 Summary and conclusion

By investigating the transport of thermo-thickening associative polymers with varying associative content in capillary tubes (of fixed dimensions) and porous medias of different properties and dimensions, the following conclusions could be drawn:

- As expected, thermo-thickening was much stronger in the porous media than in the capillary tubes and increased with increasing content of the associating polymer, salinity, and total concentration. For the TAP with the lowest associative content, the A06-polymer the lack of ability to thermo-thicken at a concentration of 1000 ppm was restored by increasing the total concentration to 2700 ppm.
- For those of our system where thermo-thickening was observed, the onset of thermo-thickening was below 60 °C and above 20 °C. The temperature steps for the 1000 ppm A10 system in 3xSSW revealed that thermo-thickening occurred between 40 and 60 °C. As it is believed that higher salinity decreases the onset temperature, it is reasonable to believe that the onset temperature for the weaker systems will also be above 40 °C, but closer to 60 °C than 3xSSW-systems.
- For three of our systems (2700 ppm A06 in SSW, and 1000 ppm A10 in SSW and in3xSSW) signs of weak thermo-thickening was also detected in the capillary tubes.
- The build-up of the associative resistance to flow to steady state resistance factor was delayed compared

to the polymer front by several pore volumes. One may suspect that the delay is linked to the concentration of associative polymer species (polymer concentration  $\times$  associative content), that is; either higher concentration or higher associative content will give a faster response. This agrees with Reichenbach-Klinke et al. [25], who reported that the impairment front ( $\propto$ [PV delay]<sup>-1</sup>), increases with increasing concentration, associative content and molecular weight, an effect which was later successfully modelled by Lohne et al. [20]. The absence of cleaning the cores between experiments in the current work prohibits a strong conclusion in this regard.

- The resistance to flow increased with decreasing shear-rate, but for the weak system, the associative resistance to flow broke down at very low shear rate, possible through the formation of intramolecular association which was not sufficiently disturbed at low rates to form new intermolecular association.
- When the core length was increased, from 7 to 76 cm, a system with a more pronounced thickening ability was needed to achieve a homogenous response over the entire core length. This was achieved by tripling the salinity of the brine for 1000 ppm A10 polymer.
- Both the build-up of resistance to flow, the return to traditional polymer behavior when the system was cooled down and clean-up time with brines were very slow processes, where the behavior in neighboring sections were strongly coupled.
- Using a front core, below the temperature for thermo-thickening, demonstrated that there is no consumption of the ability to create resistance to flow, when the polymer is not hydrophobically associating.

The work shows that by replacing a regular EOR polymer by an associative polymer it will be possible to (i) significantly alter the mobility ratio and sweep efficiency, and (ii) achieve low mobility reduction and good injectivity through the cold injection area. This work also shows that thermo-thickening is not an in-let filtration effect but indeed takes place in-depth. To achieve the same in-depth mobility reduction by using regular EOR polymers, the polymer concentration (and cost) is to be increased significantly – with negative impact on the polymer injectivity.

**Acknowledgements** The authors acknowledge Herbert Hommer, Roland Reichenbach-Klinke, and Karin Eberius for their in-put and continued support, BASF for supplying the polymers, and the Research Council of Norway and the industry partners, ConocoPhillips Skandinavia AS, Aker BP ASA, Vår Energi AS, Equinor ASA, Neptune Energy Norge AS, Lundin Norway AS, Halliburton AS, Schlumberger Norge AS, and Wintershall DEA, of The National IOR Centre of Norway for support.

**Authors' contributions** All authors contributed to the study conception and design. DS was main responsible for material preparation, AS was main responsible for data collection and analysis. The first draft of the manuscript was written by SMÅ and all authors commented on previous versions of the manuscript. All authors read and approved the final manuscript.

**Funding** The work is part of a project that is funded by The National IOR Centre of Norway. The National IOR Centre is funded by the Research council of Norway and the industry partners of The National IOR Centre of Norway: ConocoPhillips Skandinavia AS, Aker BP ASA, Vår Energi AS, Equinor ASA, Neptune Energy Norge AS, Lundin Norway AS, Halliburton AS, Schlumberger Norge AS, and Wintershall DEA.

**Data availability** Partly available on request.

**Code availability** Not applicable.

**Declaration**

**Conflict of interest** The authors have not disclosed any competing interests.

**Open Access** This article is licensed under a Creative Commons Attribution 4.0 International License, which permits use, sharing, adaptation, distribution and reproduction in any medium or format, as long as you give appropriate credit to the original author(s) and the source, provide a link to the Creative Commons licence, and indicate if changes were made. The images or other third party material in this article are included in the article's Creative Commons licence, unless indicated otherwise in a credit line to the material. If material is not included in the article's Creative Commons licence and your intended use is not permitted by statutory regulation or exceeds the permitted use, you will need to obtain permission directly from the copyright holder. To view a copy of this licence, visit <http://creativecommons.org/licenses/by/4.0/>.

## References

1. Askarinezhad R, Hatzignatiou DG, Stavland A (2018) Core-based evaluation of associative polymers as enhanced oil recovery agents in oil-wet formations. *J Energy Resour Technol* 140(3)
2. Åsen SM, Stavland A, Strand D, Hiorth A (2019) An experimental investigation of polymer mechanical degradation at the centimeter and meter scale. *SPE J* 24(04):1–700
3. Bokias G, Hourdet D, Iliopoulos I (2000) Positively charged amphiphilic polymers based on poly (N-isopropylacrylamide): Phase behavior and shear-induced thickening in aqueous solution. *Macromolecules* 33(8):2929–2935
4. Cannella WJ, Huh C, Seright RS (1988) Prediction of Xanthan rheology in porous media. *Soc Pet Eng*. <https://doi.org/10.2118/18089-MS>
5. Cao PF, Mangadlao JD, Advincula RC (2015) Stimuli-responsive polymers and their potential applications in oil-gas industry. *Polym Rev* 55(4):706–733
6. Chauveteau G, Sorbie KS (1991) *Mobility control by polymers* (Vol 33). Elsevier Science Publishers, Amsterdam
7. Du H, Wickramasinghe R, Qian X (2010) Effects of salt on the lower critical solution temperature of poly

- (N-isopropylacrylamide). *J Phys Chem B* 114(49):16594–16604. <https://doi.org/10.1021/jp105652c>
8. Didari H, Aghdasinia H, Hosseini MS, Ebrahimi F, Sahimi M (2020) Identifying the optimal path and computing the threshold pressure for flow of bingham fluids through heterogeneous porous media. *Transp Porous Media* 135(3):779–798
  9. Dupuis G, Rousseau D, Tabary R, Grassl B (2011) Flow of hydrophobically modified water-soluble-polymer solutions in porous media: New experimental insights in the diluted regime. *SPE J* 16(01):43–54. <https://doi.org/10.2118/129884-PA>
  10. Durand A, Hourdet D (1999) Synthesis and thermoassociative properties in aqueous solution of graft copolymers containing poly (N-isopropylacrylamide) side chains. *Polymer* 40(17):4941–4951
  11. Durand A, Hourdet D (2000) Thermoassociative graft copolymers based on poly (N-isopropylacrylamide): Relation between the chemical structure and the rheological properties. *Macromol Chem Phys* 201(8):858–868
  12. Gathier F, Rivas C, Lauber L, Thomas A (2020) Offshore polymer EOR injection philosophies, constraints and solutions. In: SPE improved oil recovery conference. Society of Petroleum Engineers
  13. Grinberg VY, Burova TV, Grinberg NV, Dubovik AS, Papkov VS, Khokhlov AR (2015) Energetics of LCST transition of poly (ethylene oxide) in aqueous solutions. *Polymer* 73:86–90. <https://doi.org/10.1016/j.polymer.2015.07.032>
  14. Hourdet D, L'allet F, Audebert R (1994) Reversible thermothickening of aqueous polymer solutions. *Polymer* 35(12):2624–2630
  15. Israelachvili, J. N.: Intermolecular and surface forces. Academic press, 381–405 (2011)
  16. L'allet F, Maroy P, Hourdet D, Audebert R (1997) Reversible thermoassociation of water-soluble polymers. *Revue de l'Institut Français du Pétrole* 52(2):117–128
  17. Langlotz B, Reichenbach-Klinke R, Spindler C, Wenzke B (2010) Method for oil recovery using hydrophobically associating polymers. Patent pending. European patent No. 2 643 423 B1. European Patent Office
  18. Leblanc T, Braun O, Thomas A, Divers T, Gaillard N, Favero C (2015) Rheological properties of stimuli-responsive polymers in solution to improve the salinity and temperature performances of polymer-based chemical enhanced oil recovery technologies. In: SPE asia pacific enhanced oil recovery conference. Society of Petroleum Engineers
  19. Lohne A, Nødland O, Stavland A, Hiorth A (2017) A model for non-Newtonian flow in porous media at different flow regimes. *Comput Geosci* 21(5–6):1289–1312
  20. Lohne A, Stavland A, Reichenbach-Klinke R (2019) Modeling of associative polymer flow in porous medium. In: IOR 2019–20th European symposium on improved oil recovery, vol 1, 1–28. European Association of Geoscientists & Engineers
  21. Lopez X, Valvatne PH, Blunt MJ (2003) Predictive network modeling of single-phase non-Newtonian flow in porous media. *J Colloid Interface Sci* 264(1):256–265
  22. Maerker JM (1975) Shear degradation of partially hydrolyzed polyacrylamide solutions. *Soc Petrol Eng J* 15(04):311–322
  23. Nouri HH, Root PJ (1971) A study of polymer solution rheology, flow behavior, and oil displacement processes. In: Fall meeting of the society of petroleum engineers of AIME. Society of Petroleum Engineers
  24. Palmer TL, Baardsen G, Skartlien R (2018) Reduction of the effective shear viscosity in polymer solutions due to crossflow migration in microchannels: effective viscosity models based on DPD simulations. *J Dispersion Sci Technol* 39(2):190–206
  25. Reichenbach-Klinke R, Stavland A, Strand D, Langlotz B, Brodt G (2016) Can associative polymers reduce the residual oil saturation?. In: SPE EOR conference at oil and gas West Asia. Society of Petroleum Engineers
  26. Reichenbach-Klinke R, Zimmermann T, Stavland A, Strand D (2018) Temperature-switchable polymers for improved oil recovery. In: SPE Norway one day seminar. Society of Petroleum Engineers
  27. Seright RS (1983) The effects of mechanical degradation and viscoelastic behavior on injectivity of polyacrylamide solutions. *Soc Petrol Eng J* 23(03):475–485
  28. Seright RS, Fan T, Wavrik K, Wan H, Gaillard N, Favéro C (2011) Rheology of a new sulfonic associative polymer in porous media. *SPE Reservoir Eval Eng* 14(06):726–734
  29. Seright R, Skjevraak I (2015) Effect of dissolved iron and oxygen on stability of hydrolyzed polyacrylamide polymers. *SPE J* 20(03):433–441
  30. Sheng JJ, Leonhardt B, Azri N (2015) Status of polymer-flooding technology. *J Can Pet Technol* 54(02):116–126
  31. Sorbie KS (1991) Polymer-improved oil recovery. Blackie and Sons Ltd, Glasgow
  32. Standnes DC, Skjevraak I (2014) Literature review of implemented polymer field projects. *J Petrol Sci Eng* 122:761–775
  33. Stavland A, Jonsbraten H, Lohne A, Moen A, Giske NH (2010) Polymer flooding-flow properties in porous media versus rheological parameters. In: SPE EUROPEC/EAGE annual conference and exhibition. Society of Petroleum Engineers
  34. Stavland A, Åsen SM, Mebratu A, Gathier F (2020) Scaling of mechanical degradation of EOR-polymers: from field-scale chokes to capillary tubes. *SPE Production & Operations*
  35. Teeuw D, Hesselink FT (1980) Power-law flow and hydrodynamic behaviour of biopolymer solutions in porous media. In: SPE oil-field and geothermal chemistry symposium. Society of Petroleum Engineers
  36. Weast RC, Astle MJ (1983) CRC handbook of chemistry and physics, 63rd edn. CRC, Boca Raton, FL
  37. Zhong C, Luo P, Ye Z, Chen H (2009) Characterization and solution properties of a novel water-soluble terpolymer for enhanced oil recovery. *Polym Bull* 62(1):79–89
  38. Zhu Y, Xu Y, Huang G (2013) Synthesis and aqueous solution properties of novel thermosensitive polyacrylamide derivatives. *J Appl Polym Sci* 130(2):766–775. <https://doi.org/10.1002/app.39192>

**Publisher's Note** Springer Nature remains neutral with regard to jurisdictional claims in published maps and institutional affiliations.